JOURNAL OF APPLIED CRYSTALLOGRAPHY

ISSN 1600-5767

Detection of an ordered-structure fraction in amorphous silicon

Xiao-Dong Wang,* Bo Chen, Hai-Feng Wang, Xin Zheng, Shi-Jie Liu, Jun-Bo Wang, Bo Li, Shan-Meng Yu and Zhong-Xu Cui

Changchun Institute of Optics, Fine Mechanics and Physics, Chinese Academy of Sciences, Changchun, 130033, People's Republic of China. *Correspondence e-mail: wangxiaodong@ciomp.ac.cn

Received 13 June 2015
Accepted 11 February 2016

Edited by A. J. Allen, National Institute of Standards and Technology, Gaithersburg, USA

Keywords: amorphous silicon; medium-range order; continuous random networks; spectroscopic ellipsometry.

Amorphous silicon (a-Si) films were prepared by radio frequency magnetron sputtering. Spectroscopic ellipsometry (SE) was utilized to detect an ordered-structure fraction in a-Si. The SE analysis of a-Si films with different thicknesses (7.0–140.0 nm) demonstrates that no more than 2.81% of medium-range order exists in the samples, and interestingly, there is a thickness dependence of optical constants for a-Si in the range of 1.5–5.0 eV.

1. Introduction

Amorphous silicon (a-Si) film is an important material used in second-generation solar cells (Astakhov *et al.*, 2009) and optical mulitilayer films (Wang *et al.*, 2007). All of these applications motivate the extensive investigation of a-Si films. Traditionally, the structure of a-Si has been modeled as a continuous random network (CRN). However, Phillips *et al.* (1987) observed crystalline clusters in a-Si films by high-resolution transmission electron microscopy. Their observations support a submicrocrystalline model for the structure of a-Si. Gibson and co-workers (Gibson *et al.*, 2010; Voyles *et al.*, 2001; Gibson & Treacy, 1997; Treacy *et al.*, 1998, 2000) believed that there are strained, topologically crystalline grains (1–2 nm) in tetrahedral amorphous semiconductor films. In 2012, Treacy & Borisenko (2012*a*) and Gibson (2012) published papers in *Science*, systemically elucidating the existence of medium-range order (MRO) in tetrahedral amorphous semiconductor films and challenging the traditional CRN model for amorphous materials. Subsequently, Roorda & Lewis (2012) commented on Treacy and Borisenko's results and argued that the paracrystalline model disagrees with high-resolution X-ray data, whereas the agreement with fluctuation electron microscopy is at best qualitative. Later, Treacy & Borisenko (2012*b*) gave a quick response to Roorda's comment. Thus, the existent of MRO in a-Si is still under debate.

Tomlin and co-workers (Tomlin *et al.*, 1976; Thutupalli & Tomlin, 1977) studied the optical properties of, respectively, a-Ge and a-Si on the basis of the Mott–Davis model (Mott & Davis, 1979), and described the band gap of as-deposited and post-annealing samples. In addition, it has been revealed that the band gap of a-Ge exhibits a distinct thickness effect, and it was believed that the void fraction, amorphous effect and one-dimensional quantum confinement (ODQC) effect can be used to interpret the thickness dependence of the band gap (Pilione *et al.*, 1987; Goh *et al.*, 2010). Recently, based on the observation of MRO in tetrahedral amorphous semiconductor films, our group proposed a Mott–Davis paracrystalline model

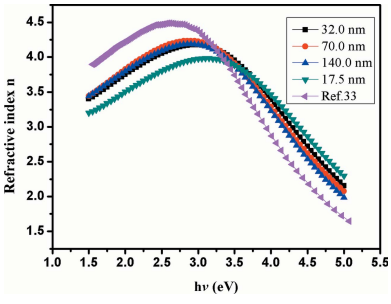

Table 1
SE analysis results of a-Si films with ordered structure based on the MRO model.

Values in parentheses are the uncertainties on the least significant digits.

d† (nm)	d_1 (nm)	d_2 (nm)	a-Si (%)	c-Si (%)	E_g (eV)	$\varepsilon_1(\infty)$	A (eV)	E_0 (eV)	C (eV)	χ^2
7.0	6.82 (15)	4.72 (26)	87.17 (621)	0.86 (20)	2.077 (23)	1.55 (9)	210 (18)	3.95 (4)	5.17 (14)	0.238
10.5	102.00 (22)	3.33 (19)	93.54 (553)	1.50 (23)	2.131 (16)	2.10 (11)	161 (14)	4.32 (4)	6.21 (7)	0.221
17.5	17.17 (34)	0.58 (6)	95.48 (541)	2.81 (33)	1.610 (16)	1.07 (6)	127 (11)	4.03 (3)	3.28 (3)	0.188
32.0	29.66 (21)	1.76 (12)	94.01 (713)	0.05 (15)	1.505 (18)	1.16 (10)	138 (16)	2.94 (3)	3.59 (2)	0.366
70.0	64.88 (16)	1.17 (10)	91.33 (801)	0.00 (14)	1.516 (12)	1.06 (9)	149 (20)	3.71 (1)	2.88 (3)	0.340
140.0	132.71 (66)	1.20 (18)	90.88 (1101)	0.00 (17)	1.434 (16)	1.12 (14)	146 (27)	3.73 (2)	2.77 (5)	1.229

† The film thickness is characterized by a NEWVIEW 6K optical profiling system.

combined with the ODQC effect to interpret the thickness dependence of the band gap (Wang *et al.*, 2013). In this paper, we aim to determine whether there is MRO in a-Si films by the spectroscopic ellipsometry (SE) method and to determine whether there is a thickness dependence of MRO for a-Si.

2. Experiments and methods

a-Si films were deposited by a radio frequency magnetron sputtering deposition machine with a working gas of Ar (99.999%). The Si target has a purity of 99.999%. The base pressure of the chamber was 8.0×10^{-5} Pa, and the working pressure was 0.1 Pa. The deposition power was kept constant at 250 W. The a-Si films were deposited onto a fused silica substrate with no heating. The film thickness was monitored only by time owing to the stable deposition rate of the sputtering method. All film samples were optically characterized after one month of aging.

The film thickness and surface roughness were measured by a NEWVIEW 6K optical profiling system (ZYGO) with 10× objective. The reflectance (R) and transmission (T) of the thin films were characterized by a Lambda 950 spectrophotometer (PerkinElmer), with the incident angle fixed at 8°. The film structures were analyzed by SE (UVISEL, HORIBA Scientific); this measurement was conducted at an incident angle of 70° and the photon energy range was 1.5–5.0 eV. The thickness of our substrate was 1.5 mm, and a piece of paper was used to block the incoherent backside reflections.

3. Results and discussion

We employed SE to determine the volume fraction of MRO in our samples. In the SE analysis, the Tauc–Lorentz model is used to describe the optical functions of the a-Si layer in the spectral fitting because this model (Oever *et al.*, 2007; Jellison & Modine, 1996) has been demonstrated to provide an excellent characterization of dielectric function for amorphous semiconductor films.

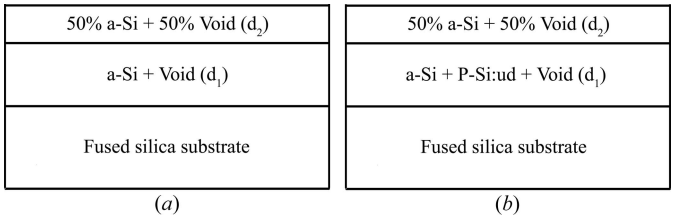

Figure 1
The four-phase models without ordered structure (a) and with ordered structure (b).

In this model, the imaginary part of the dielectric function is written as

$$\varepsilon_2(E) = \begin{cases} \left[\dfrac{AE_0C(E-E_g)^2}{(E^2-E_0^2)^2 + C^2E^2}\,\dfrac{1}{E}\right], & E > E_g, \\ 0, & E \le E_g, \end{cases} \quad (1)$$

where A, C, E_0 and E_g are all in units of energy. A is the amplitude, C is the broadening term, E_0 is the peak transition energy and E_g is the optical band gap (Jellison & Modine, 1996).

The real part of the dielectric function is obtained from Kramers–Kronig integration of $\varepsilon_2(E)$ and is given by

$$\varepsilon_1(E) = \varepsilon_1(\infty) + \frac{2}{\pi} P \int_{E_g}^{\infty} \frac{\xi\varepsilon_2(\xi)}{\xi^2 - E^2}\,\mathrm{d}\xi, \quad (2)$$

where P is the Cauchy principal part of the integral, and $\varepsilon_1(\infty)$ is another fitting parameter (Jellison & Modine, 1996).

Fig. 1 shows the four-phase model (air/surface-roughness layer/Si layer/fused-silica substrate) utilized in the SE analysis of the a-Si films. The phases of the roughness layer and Si layer are described by the Bruggeman effective medium approximation (Bruggeman, 1935). Traditionally, each fraction of the two components in the roughness layer is fixed to be 50%. A fine crystalline grain model (Hazra *et al.*, 2004) is utilized to describe the Si layer (as shown in Fig. 1b). The main difference between Figs. 1(a) and 1(b) lies in the Si layer: there is a P-Si:ud phase (small grains) in Fig. 1(b) besides the a-Si phase and Void. P-Si:ud is adopted from the work of Jellison *et al.* (1993), and it is a polycrystalline film with fine grains. For convenience, the model depicted in Fig. 1(a) is named the CRN model and that in Fig. 1(b) is called the MRO model. A, C, E_0, E_g, $\varepsilon_1(\infty)$, d_1, d_2 and the fraction of components in the Si layer are the fitting parameters in the SE analysis.

Tables 1 and 2 demonstrate the SE analysis results for the a-Si films based on the MRO model (with ordered structure) and CRN model (without ordered structure), respectively. The

Table 2
SE analysis results of a-Si films without ordered structure based on the CRN model.

Values in parentheses are the uncertainties on the least significant digits.

d† (nm)	d_1 (nm)	d_2 (nm)	a-Si (%)	E_g (eV)	$\varepsilon_1(\infty)$	A (eV)	E_0 (eV)	C (eV)	χ^2
7.0	7.15 (12)	4.93 (25)	99.63 (821)	2.094 (22)	1.58 (9)	180 (19)	3.98 (4)	5.19 (14)	0.240
10.5	10.62 (32)	3.55 (19)	91.98 (592)	2.164 (14)	1.99 (13)	178 (17)	4.27 (5)	6.13 (7)	0.231
17.5	18.09 (34)	0.07 (2)	92.61 (525)	1.607 (16)	1.20 (6)	130 (11)	4.01 (3)	3.04 (3)	0.196
32.0	29.65 (21)	1.77 (12)	95.28 (799)	1.505 (17)	1.15 (9)	136 (17)	3.83 (3)	2.92 (6)	0.363
70.0	64.89 (15)	1.15 (9)	93.54 (816)	1.516 (12)	1.08 (9)	144 (19)	3.71 (1)	2.88 (3)	0.338
140	132.81 (64)	1.15 (16)	99.26 (1352)	1.433 (15)	1.15 (12)	127 (26)	3.73 (2)	2.77 (5)	1.220

† The film thickness is characterized by a NEWVIEW 6K optical profiling system.

thickness d of the a-Si films was obtained using the optical profiling system, and the error is less than 0.75%. As depicted in Fig. 1, the thicknesses d_1 and d_2 in Tables 1 and 2 correspond to the a-Si layer and roughness layer, respectively, and they were derived from the SE analysis. As shown in Table 1, the maximum fraction of c-Si is 2.81%, and the MRO model shows no priority as compared to the CRN model judged by the goodness-of-fit characterized by χ^2 in the two models. In other words, there is such a low volume fraction of MRO that no significant changes of optical properties are detected by the SE method in the two models.

Two measured parameters Ψ and Δ in SE measurements are defined by equation (3):

$$\rho = r_p/r_s = \tan\psi \exp(i\Delta), \tag{3}$$

where r_p and r_s are the Fresnel coefficients of reflection for p- and s-polarization, respectively.

Fig. 2 illustrates experimental curves and fitting results of Ψ and Δ for the 17.5 nm a-Si film, the fits being based on the MRO and CRN models. The fitting results show a good agreement with the experimental curves, and it is found that the fitting results possess similar goodness-of-fit, provided that there is no more than 2.81% MRO in the MRO model. The high volume fraction of MRO may only be present in some special a-Si films, since the detailed ordering in a-Si is known to depend on the fabrication process. Substrate heating may contribute to formation of MRO in a-Si films.

SE is a powerful, very sensitive technique. However, its absolute accuracy is very difficult to determine. Other complementary methods should be employed to prove its veracity. Now three routes, including optical band gap, film thickness and optical constants, are utilized to verify the correctness of the SE results.

The optical band gap of a-Si (an indirect semiconductor) is obtained by Tauc's equation and is given by

$$(\alpha h\nu)^{1/2} = B(h\nu - E_g), \tag{4}$$

where $h\nu$ is the photon energy, B is the edge width and α is the absorption coefficient (Demichelis *et al.*, 1987; Tsao *et al.*, 2010; Banerjee & Chattopadhyay, 2005). The absorption coefficient can be derived by

$$\alpha = 4\pi k/\lambda, \tag{5}$$

where λ is the wavelength and k is the extinction coefficient, which can be obtained from R and T of the a-Si films *via* the *Optilayer* software.

Fig. 3 demonstrates a Tauc plot of $(\alpha h\nu)^{1/2}$ *versus* photon energy $h\nu$ for a-Si films based on the α values derived from R and T. The optical band gap E_g is obtained by extrapolation of the linear portion at $(\alpha h\nu)^{1/2} = 0$. For brevity, only the Tauc plots for the 32.0 and 70.0 nm a-Si films are drawn. Table 3

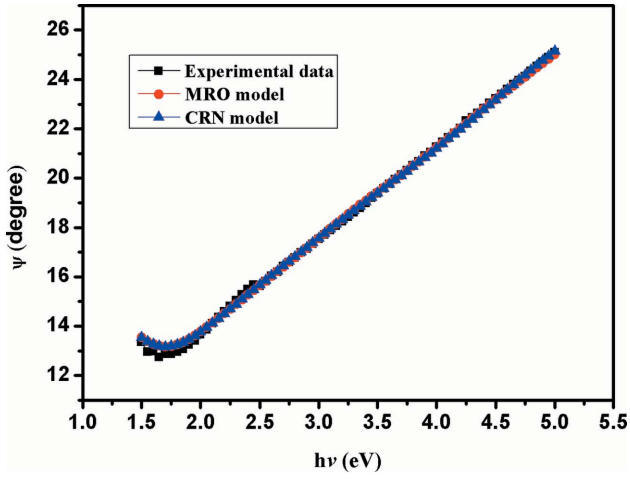

(*a*)

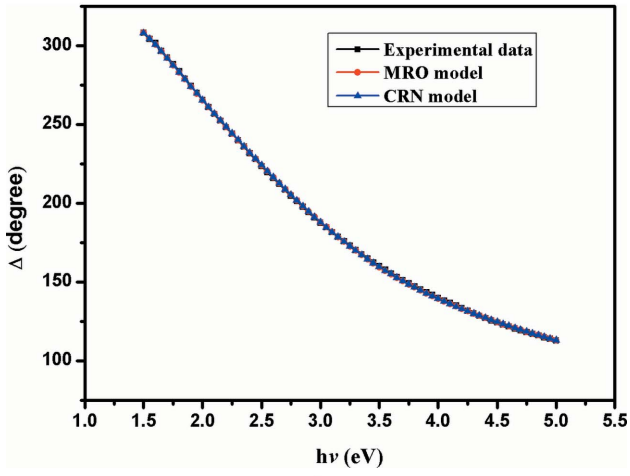

(*b*)

Figure 2
Experimental results and fitting data of Ψ (*a*) and Δ (*b*) for the 17.5 nm a-Si film.

Table 3
Band gap of 7.0–140.0 nm a-Si films derived from Tauc plots and SE analysis.

Thickness d (nm)	$E_{g,opt}$ (eV)	E_g (with MRO) (eV)	E_g (without MRO) (eV)
7.0	1.898	2.077 (23)	2.094 (22)
10.5	1.969	2.131 (16)	2.164 (14)
17.5	1.736	1.610 (16)	1.607 (16)
32.0	1.749	1.505 (18)	1.505 (17)
70.0	1.692	1.516 (12)	1.516 (12)
140.0	1.400	1.434 (16)	1.433 (15)

summarizes values of the band gap for 7.0–140.0 nm a-Si films, obtained from Tauc plots, and film thickness d, obtained using the optical profiling system. As shown in Table 3, the $E_{g,opt}$ optical band gap obtained from the Tauc plots varies from 1.400 to 1.969 eV, and it has a 99.9% confidence interval. The difference in band gap between Tauc plots and SE analysis is small (0.033–0.244 eV), which reveals that the SE analysis results are credible.

Table 4 summarizes the film thicknesses (32.0, 70.0 and 140.0 nm) obtained by the optical profiling system, *Optilayer* software fitting and SE analysis. D denotes the discrepancy value in the *Optilayer* software fitting. The difference in thickness between these methods is less than 7.34%, which, again, indicates that the analysis results of SE are credible.

For brevity, Fig. 4 only demonstrates optical constants of the 32.0–140.0 nm a-Si films. The peaks of refractive index and extinction coefficient shift towards longer wavelength with increasing of film thickness, and the values of refractive index and extinction coefficient also increase as film thickness increases. Similar phenomena were observed in thin metal films (Amotchkina *et al.*, 2011; Lehmuskero *et al.*, 2007). The reason for this phenomenon is beyond the scope of this article and will be discussed elsewhere. The optical constant of a-Si reported by the Center for Nanolithography Research of Rochester Institute of Technology (RIT) was drawn in Fig. 4

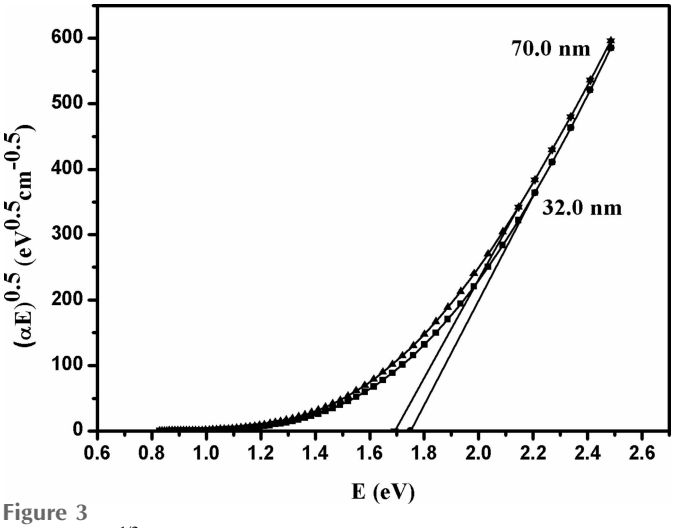

Figure 3
Plot of $(\alpha E)^{1/2}$ *versus* photon energy (E) for the 32.0 and 70.0 nm a-Si films.

Table 4
Thickness of a-Si films determined by the optical profiling system, *Optilayer* software and SE analysis.

Thickness (profiling system)		d (*Optilayer*) (nm)		d (with MRO) (nm)		d (without MRO) (nm)	
d (nm)	error	d (nm)	D	d (nm)	χ^2	d (nm)	χ^2
32.0	<0.75%	34.18	5.392	29.66 (21)	0.366	29.65 (21)	0.363
70.0		65.94	5.190	64.88 (16)	0.340	64.89 (15)	0.338
140.0		133.85	6.257	132.71 (66)	1.229	132.81 (64)	1.220

for comparison (denoted Ref.33 in the figure). The shape and trend of optical constants of a-Si films characterized by the SE method are similar to those from RIT, which demonstrates that our SE analysis results are reliable.

From the analysis of the difference in band gap, film thickness and optical constants between SE and other characterization methods, it is believed that our SE analysis results are reliable. Thus, in conclusion, it is found that there is little MRO in our a-Si films. In other words, CRNs are dominant in our a-Si samples.

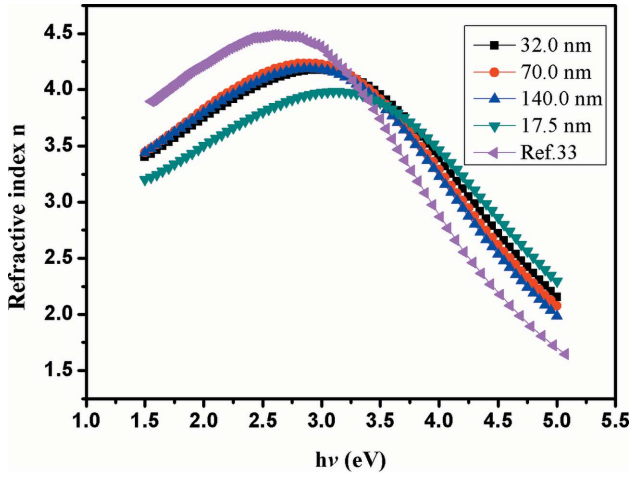

(*a*)

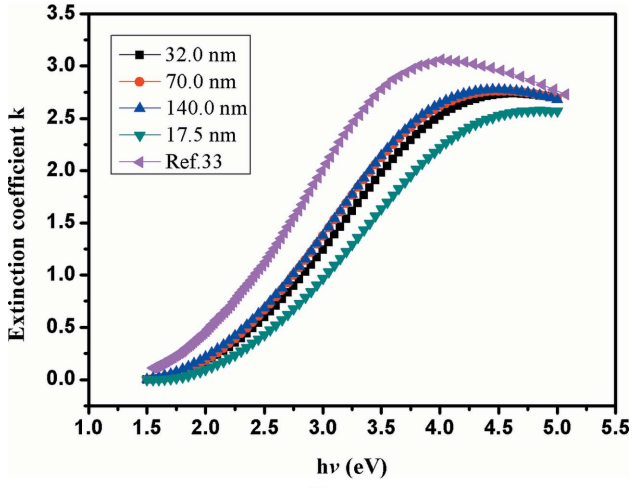

(*b*)

Figure 4
Optical constants of 32.0–140.0 nm a-Si films: (*a*) refractive index and (*b*) extinction coefficient. The data are derived from an SE analysis based on the CRN model.

4. Summary

Our SE analysis indicates that CRNs are dominant in our a-Si films, and the volume fraction of MRO in our samples is no more than 2.81%, which disagrees with the argument (50% of MRO) of Gibson. In addition, the peaks of refractive index and extinction coefficient of a-Si shift towards longer wavelength with increasing film thickness, and the values of refractive index and extinction coefficient also increase as film thickness increases.

References

Amotchkina, T. V., Janicki, V., Sancho-Parramon, J., Tikhonravov, A. V., Trubetskov, M. K. & Zorc, H. (2011). *Appl. Opt.* **50**, 1453–1464.

Astakhov, O., Carius, R., Finger, F., Petrusenko, Y., Borysenko, V. & Barankov, D. (2009). *Phys. Rev. B*, **79**, 104205.

Banerjee, A. N. & Chattopadhyay, K. K. (2005). *J. Appl. Phys.* **97**, 084308.

Bruggeman, D. A. G. (1935). *Ann. Phys.* **416**, 636–664.

Demichelis, F., Kaniadakis, G., Tagliaferro, A. & Tresso, E. (1987). *Appl. Opt.* **26**, 1737–1740.

Gibson, J. M. (2012). *Science*, **335**, 929–930.

Gibson, J. M. & Treacy, M. M. J. (1997). *Phys. Rev. Lett.* **78**, 1074–1077.

Gibson, J. M., Treacy, M. M. J., Sun, T. & Zaluzec, N. J. (2010). *Phys. Rev. Lett.* **105**, 125504.

Goh, E. S. M., Chen, T. P., Sun, C. Q. & Liu, Y. C. (2010). *J. Appl. Phys.* **107**, 024305.

Hazra, S., Sakata, I., Yamanaka, M. & Suzuki, E. (2004). *Phys. Rev. B*, **69**, 235204.

Jellison, G. E., Chisholm, M. F. Jr & Gorbatkin, S. M. (1993). *Appl. Phys. Lett.* **62**, 3348–3350.

Jellison, G. E. & Modine, F. A. (1996). *Appl. Phys. Lett.* **69**, 371–374.

Lehmuskero, A., Kuittinen, M. & Vahimaa, P. (2007). *Opt. Express*, **15**, 10744–10752.

Mott, N. F. & Davis, E. A. (1979). *Electronic Processes in Non-crystalline Solids.* Oxford: Clarendon Press.

Oever, P. J. van den, van de Sanden, M. C. M. & Kessels, W. M. M. (2007). *J. Appl. Phys.* **101**, 123529.

Phillips, J. C., Bean, J. C., Wilson, B. A. & Ourmazd, A. (1987). *Nature*, **325**, 121–125.

Pilione, L. J., Vedam, K., Yehoda, J. E., Messier, R. & McMarr, P. J. (1987). *Phys. Rev. B*, **35**, 9368–9371.

Roorda, S. & Lewis, L. J. (2012). *Science*, **338**, 1539.

Thutupalli, G. K. M. & Tomlin, S. G. (1977). *J. Phys. C*, **10**, 467–477.

Tomlin, S. G., Khawaja, E. & Thutupalli, G. K. M. (1976). *J. Phys. C Solid State Phys.* **9**, 4335–4347.

Treacy, M. M. J. & Borisenko, K. B. (2012*a*). *Science*, **335**, 950–953.

Treacy, M. M. J. & Borisenko, K. B. (2012*b*). *Science*, **338**, 1539.

Treacy, M. M. J., Gibson, J. M. & Keblinski, P. J. (1998). *J. Non-Cryst. Solids*, **231**, 99–110.

Treacy, M. M. J., Voyles, P. M. & Gibson, J. M. (2000). *J. Non-Cryst. Solids*, **266–269**, 150–155.

Tsao, C. Y., Weber, J. W., Campbell, P., Conibeer, G., Song, D. & Green, M. A. (2010). *Solar Energy Mater. Solar Cells*, **94**, 1501–1505.

Voyles, P. M., Zotov, Z., Nakhmanson, S. M., Drabold, D. A., Gibson, J. M., Treacy, M. M. J. & Keblinski, P. (2001). *J. Appl. Phys.* **90**, 4437–4451.

Wang, X. D., Wang, H. F., Chen, B., Li, Y. & Ma, Y. (2013). *Appl. Phys. Lett.* **102**, 202102.

Wang, Z. *et al.* (2007). *Appl. Phys. Lett.* **90**, 031901.